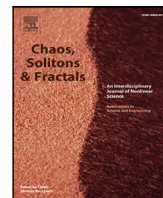


ULRR

Efficient mass-preserving finite volume approach for the rennet-induced coagulation equation

Item Type	Article
Authors	Singh, Mehakpreet;Sriwastav, Nikhil;Shardt, Orest
Citation	Chaos, Solitons & Fractals 181, 114692
Publisher	Elsevier
Download date	2026-03-17 08:31:15
Item License	https://creativecommons.org/licenses/by-nc-sa/4.0/
Link to Item	https://doi.org/10.34961/researchrepository-ul.25721526



Efficient mass-preserving finite volume approach for the rennet-induced coagulation equation

Mehakpreet Singh^{a,b,*}, Nikhil Sriwastav^c, Orest Shardt^{b,d}

^a Mathematics Applications Consortium for Science and Industry (MACSI), Department of Mathematics & Statistics, University of Limerick, Limerick, V94 T9PX, Ireland

^b Dairy Processing Technology Centre, University of Limerick, Limerick, V94 T9PX, Ireland

^c Department of Mathematics and Scientific Computing, Madan Mohan Malaviya University of Technology, Gorakhpur 273010, India

^d Bernal Institute, Department of Chemical Sciences, University of Limerick, Limerick, V94 T9PX, Ireland

ARTICLE INFO

Keywords:

Dairy processing
Rennet coagulation
Cheese manufacturing
Integro-partial differential equations
Population balance equation
Finite volume scheme

ABSTRACT

The coagulation of casein micelles caused by enzymes is a critical step in the dairy industry for cheese manufacture. During enzymatic coagulation of milk, three processes occur: enzymic proteolysis, coagulation, and gelation. This study presents the first numerical approach based on a finite volume scheme for describing the enzyme-induced coagulation of casein micelles. The finite volume scheme is mainly concerned with ensuring mass conservation and developed on the assumption that the particles are concentrated on the mean of each cell of the discretization. The key advantages of the new technique are its simple mathematical formulation and its robustness that allow it to be implemented on any type of grid and tailored to different coagulation kernels. The accuracy of the new approach is compared with newly derived analytical results for several gelling and non-gelling coagulation kernels. The comparison demonstrates that the new approach closely matches the exact results. In order to analyse the convergence behaviour of different order moments, various refined non-uniform grids have been taken into consideration.

1. Introduction

The coagulation of milk induced by enzymes is a well-known phenomenon that is the basis for manufacturing many cheeses. The addition of milk-clotting enzyme to milk initiates a proteolytic interaction [1–3] with casein micelles. During this process, various sized casein micelles in the form of colloidal protein clusters are formed in the system (diameter lies between 50 and 500 nm). During enzymatic coagulation of milk, three different phases occur. Out of the three stages, the first two stages are of our interest for the current study. In the first stage, unstable micelles of paracasein (P_1) of volume x are formed from casein micelles (C) in the presence of enzyme (E) by the splitting off of glycomacropetides (GMPs) at a rate v . The graphical representation of the first stage is depicted in Fig. 1 and a detailed description can be found in [4,5].

In the second stage of the enzymatic coagulation of milk, the coagulation of unstable micelles of paracasein of volumes $x-x'$ and x' takes place at an aggregating rate $\beta(x-x', x')$ (a graphical representation of the second stage is provided in Fig. 2). Coagulation is a unifying process by virtue of which the formation of larger particles takes place in the system from the merging of two or more particles. The coagulation

process reduces the number of paracasein micelles in the system, whereas the total mass in the system remain unaltered. Coagulation processes have been studied and employed for solving many applications including pharmaceutical sciences [6], chemical engineering [7, 8], nano-particle physics [9], biology [10] and thermodynamics [11].

1.1. Rennet-induced coagulation equation

The evolution of the number density function $f(x, t)$ of the paracasein micelles having volume $x \in \mathfrak{R}^+$ at time $t \geq 0$ subject to the enzymatic coagulation process is governed by an integro-partial differential equation that can be written as:

$$\frac{\partial f(x, t)}{\partial t} = K_1 g(x, 0)e^{-K_1 t} + \frac{1}{2} \int_0^x \beta(x', x-x') f(x-x', t) f(x', t) dx' - \int_0^\infty \beta(x, x') f(x, t) f(x', t) dx', \quad (1)$$

with the initial conditions $g(x, 0) = g^{in}(x)$ for the casein micelles and $f(x, 0) = f^{in}(x)$ for paracasein micelles with $x \in]0, \infty[$. Here, the first expression on the right hand side of Eq. (1) represents the primary phase of the enzymatic coagulation process which is considered to

* Corresponding author at: Dairy Processing Technology Centre, University of Limerick, Limerick, V94 T9PX, Ireland.
E-mail addresses: Mehakpreet.Singh@ul.ie (M. Singh), Orest.Shardt@ul.ie (O. Shardt).

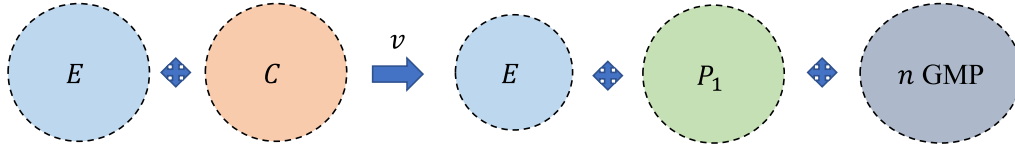


Fig. 1. Depiction of first stage of enzymatic coagulation of milk.

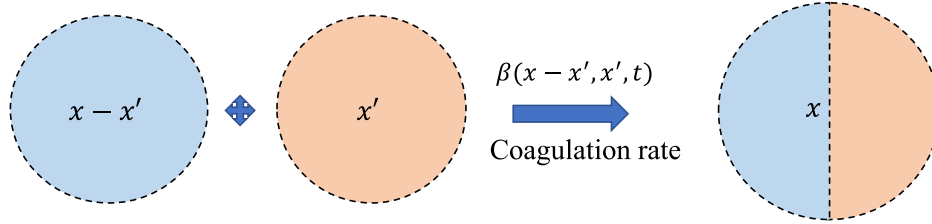


Fig. 2. Graphical representation of the second stage of enzymatic coagulation of milk.

be described by first-order kinetics and K_1 is the rate constant for proteolysis. The rate is assumed to be independent of the micelle size. This term follows from the solution to

$$\frac{\partial g(x, t)}{\partial t} = -K_1 g(x, t) \quad (2)$$

which is $g(x, t) = g(x, 0)e^{-K_1 t}$. The rate of generation of paracasein micelles is $-\frac{\partial g}{\partial t} = K_1 g(x, 0)e^{-K_1 t}$. The second term on the right side of (1) defines the formation of larger paracasein micelles having volume x due to the merging of paracasein micelles of volume $x - x'$ and x' . The third term describes the elimination of paracasein micelles of volume x with those of volume x' . Moreover, the coagulation kernel $\beta(x, x')$ denotes the rate at which two micelles of volumes x and x' combine. This coagulation kernel is non-negative and symmetric with respect to the micelle size, that is, $\beta(x, x') = \beta(x', x)$.

1.2. Literature review and motivation

The second stage of the enzymatic coagulation process, described by (1), has been subjected to numerous studies that have examined different aspects including the existence and uniqueness of solutions [12], scaling and self-similarity [13], and the gelation effect [14]. Gelation is a phase transition characterized by the coagulation equation's inability to conserve mass (or volume). However, the nonlinear behaviour of (1) restricts analytical solutions to only simple structured kernels [15–20]. Existing numerical approaches for the second stage of enzymatic coagulation process are available in literature such as method of moments [14], discrete element method [21], Lattice Boltzmann method [22], finite volume schemes [23–27], and sectional methods [28,29]. The merits and demerits of the aforementioned methods have been discussed in detail by Singh et al. [30] and references therein.

However, as per our knowledge, no analytical or numerical solutions are available for the enzymatic coagulation equation (1). In the literature, different authors (refer to [31,32] and references therein) solved the combined first two stages of enzymatic coagulation by converting it to the moment form which is given by:

$$\begin{aligned} \frac{d\mu_k(t)}{dt} &= K_1 e^{-K_1 t} \int_0^\infty x^k g(x, 0) dx \\ &+ \int_0^\infty \int_0^\infty \left[\frac{1}{2} (x + x')^k - x^k - x'^k \right] \beta(x, x') f(x, t) f(x', t) dx dx'. \end{aligned} \quad (3)$$

Here $\mu_k(t)$ denotes the k th order moment. For $k = 0$, the zeroth order moment can be captured, which provides the total number of paracasein micelles in the system. For $k = 1$ and $k = 2/3$, the

moments describe the total volume (or mass) and total surface area of paracasein micelles in the system, respectively. It is important to note that once the original equation (1) is converted into moment form (3), the information related to the number density function $f(x, t)$ is lost. However, if we solve the original equation (1) for the number density function $f(x, t)$, the moments at any time t can be easily obtained by evaluating the definition of the moments:

$$\mu_k(t) = \int_0^\infty x^k f(x, t) dx. \quad (4)$$

In this work, our aim is to develop a finite volume approach that describes the combined first two stages of enzymatic coagulation to track the number density function of the original equation (1). The finite volume approach is developed based on the assumption that the micelles are concentrated on the pivot (or representative) of the cell and focused on conserving the total mass in the system. However, it will be interesting to see the extent to which the new approach captures the zeroth and second order moments with high precision even though no specific measures have been taken for tracking these moments well. In addition, the analytical moments corresponding to different coagulation kernels will be derived in order to verify the numerical moments obtained using the finite volume approach.

The rest of content of the article is outlined as follows: the detailed derivation of the mathematical formulation of the finite volume approach for the enzymatic coagulation process (1) is presented in Section 2 along with the theoretical proof of mass conservation. In Section 3, the numerical scheme is tested against the analytical results in order to check the accuracy and efficiency of the scheme for different coagulation kernels. Next Section 4 is used to make some important remarks and conclusions related to the current study.

2. Domain discretization and finite volume scheme

In this section, let us now construct the mathematical formulation for the finite volume approach to approximating enzymatic coagulation on non-uniform grids. The formulation is derived using a non-uniform grid due to the drawbacks of uniform grids that are discussed in Section 3. Our focus is to develop a numerical method, so it is very important to fix the upper limit (∞) to a finite number, say x_{max} , in the third term on the right of Eq. (1). This limit is chosen in a way that no mass will leave the computational domain. The computational domain with the limits $x_{min} = 0$ to x_{max} is partitioned into I number of non-uniform cells as shown in Fig. 3. Suppose the lower and the upper limits of the i th cell are denoted by $x_{i-1/2}$ and $x_{i+1/2}$, respectively, where $i = \{1, 2, \dots, I\}$. The pivot of the i th cell is defined as

$$x_i = \frac{x_{i-1/2} + x_{i+1/2}}{2},$$

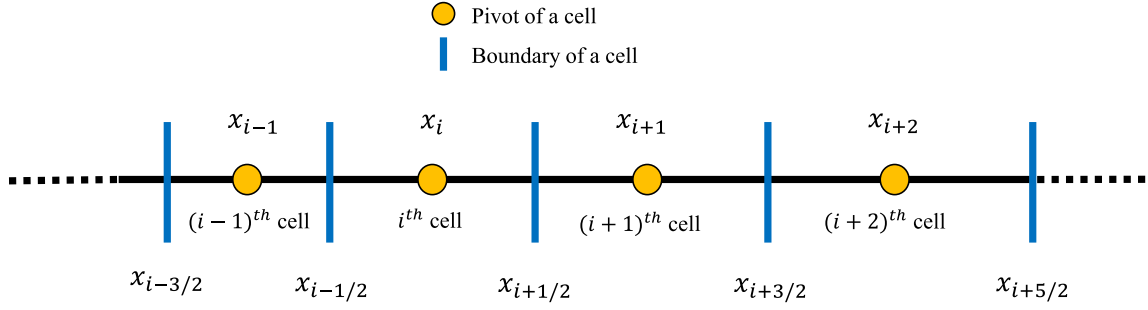


Fig. 3. Domain discretization in one dimensional space.

with $x_{i/2} = 0$ and $\Delta x_i = x_{i+1/2} - x_{i-1/2}$. For the mathematical derivation of the finite volume scheme, it is pre-assumed that all paracasein micelles formed in the system are concentrated on the pivots of the cells, that is,

$$f(x, t) = \sum_{i=1}^I N_i(t) \delta(x - x_i), \quad (5)$$

where $N_i(t) = \int_{x_{i-1/2}}^{x_{i+1/2}} f(x, t) dx$ denotes the total number of paracasein micelles in the i th cell. The idea of the finite volume scheme is to convert the integral equation (1) into a set of ODEs by substituting Eq. (5) and integrating over the i th cell; the following relation is then obtained:

$$\frac{dN_i}{dt} = S_i(t) + B_i(t) - D_i(t), \quad i = 1, 2, \dots, I. \quad (6)$$

Here the terms $S_i(t)$, $B_i(t)$ and $D_i(t)$ express the source term (due to the first coagulation phase), the total birth rate, and the total death rate of the paracasein micelles in the i th cell, respectively, and are given as

$$S_i(t) = \int_{x_{i-1/2}}^{x_{i+1/2}} K_1 g(x, 0) e^{-K_1 t} dx, \quad (7)$$

$$B_i(t) = \frac{1}{2} \int_{x_{i-1/2}}^{x_{i+1/2}} \int_0^x \beta(x - x', x') f(x - x', t) f(x', t) dx' dx, \quad (8)$$

and

$$D_i(t) = \int_{x_{i-1/2}}^{x_{i+1/2}} \int_0^{x_{max}} \beta(x, x') f(x, t) f(x', t) dx' dx. \quad (9)$$

Let us further divide the time domain into $t^{n+1} = t^n + \Delta t^n$ for $n \in \{0, \dots, N-1\}$ for some $N \in \mathbb{N}$. The average value of f at time t^n in the cell i is denoted by f_i^n which is an approximation of $f(x, t^n)$ as given in equation

$$f_i^n = \frac{1}{\Delta x_i} \int_{x_{i-1/2}}^{x_{i+1/2}} f(x, t^n) dx. \quad (10)$$

Using the aforementioned notation and expressions, the simplification of Eqs. (7), (8) and (9), Eq. (6) leads to

$$f_i^{n+1} = f_i^n + \Delta t^n \left(g(x_i, 0) K_1 \int_{t^n}^{t^{n+1}} e^{-K_1 t} dt + \frac{1}{2} \sum_{(j,k) \in \Theta^i} \beta_{j,k} f_j^n f_k^n \frac{\Delta x_j \Delta x_k}{\Delta x_i} - \sum_{j=1}^I \beta_{i,j} f_i^n f_j^n \Delta x_j \right), \quad (11)$$

where

$$\Theta^i = \{(j, k) \in \mathbb{N} \times \mathbb{N} : x_{i-1/2} < (x_j + x_k) \leq x_{i+1/2}\}, \quad i \in \{1, \dots, I\}. \quad (12)$$

Here Θ^i is a set of indices which defines the sum of micelles with volumes x_j and x_k that will fall in some i th cell after the coagulation and $\beta_{x_j, x_k} = \beta_{j,k}$. Similar to standard finite volume schemes, the current finite volume approach should satisfy mass conservation. However, the formulation (11) does not conserve the total mass in the system.

The formulation ensures mass conservation if it satisfies the following condition:

$$\mu_1(t^{n+1}) = \mu_1(t^n) + \left[e^{-K_1 t^n} - e^{-K_1 t^{n+1}} \right] \sum_{i=1}^I x_i g(x_i, 0) \Delta x_i. \quad (13)$$

One can easily prove that even though the formulation does not conserve the total mass in the system, it does conserve the zeroth order moment (total number of particles). The formulation conserves the zeroth order moment if it satisfies [33]:

$$\mu_0(t^{n+1}) = \mu_0(t^n) + \left[e^{-K_1 t^n} - e^{-K_1 t^{n+1}} \right] \sum_{i=1}^I g(x_i, 0) \Delta x_i - \frac{1}{2} \sum_{j=1}^I \sum_{k=1}^I \beta_{j,k} f_j^n f_k^n \Delta x_j \Delta x_k. \quad (14)$$

2.1. Number preservation property

Proposition 1. *The discrete formulation (11) conserves the zeroth order moment.*

Proof. Multiplying Eq. (11) by Δx_i and summing over all i , the left hand side gives the zeroth order moment ($\mu_0(t)$) at time t^{n+1} and the right hand side can be evaluated to:

$$\mu_0(t^{n+1}) = \sum_{i=1}^I f_i^n \Delta x_i + \sum_{i=1}^I g(x_i, 0) \Delta x_i K_1 \int_{t^n}^{t^{n+1}} e^{-K_1 t} dt + \Delta t^n T_1, \quad (15)$$

where

$$T_1 = \frac{1}{2} \sum_{i=1}^I \sum_{(j,k) \in \Theta^i} \beta_{j,k} f_j^n f_k^n \Delta x_j \Delta x_k - \sum_{i=1}^I \sum_{j=1}^I x_i \beta_{i,j} f_i^n f_j^n \Delta x_i \Delta x_j. \quad (16)$$

For proving the number preservation law, it is needed to prove that $T_1 = -\frac{1}{2} \sum_{j=1}^I \sum_{k=1}^I \beta_{j,k} f_j^n f_k^n \Delta x_j \Delta x_k$.

Interchanging i to j and j to k in the second term of above equation leads to

$$T_1 = \frac{1}{2} \sum_{i=1}^I \sum_{(j,k) \in \Theta^i} \beta_{j,k} f_j^n f_k^n \Delta x_j \Delta x_k - \sum_{j=1}^I \sum_{k=1}^I \beta_{j,k} f_j^n f_k^n \Delta x_j \Delta x_k. \quad (17)$$

It is worth noting that the summation $\sum_{i=1}^I \sum_{(j,k) \in \Theta^i}$ shows the combination of all cells having indices j and k that intersect with cell of index i . Therefore, it can also be written as

$$\sum_{i=1}^I \sum_{(j,k) \in \Theta^i} = \sum_{j=1}^I \sum_{k=1}^I. \quad (18)$$

This further leads to

$$T_1 = \frac{1}{2} \sum_{j=1}^I \sum_{k=1}^I \beta_{j,k} f_j^n f_k^n \Delta x_j \Delta x_k - \sum_{j=1}^I \sum_{k=1}^I \beta_{j,k} f_j^n f_k^n \Delta x_j \Delta x_k. \quad (19)$$

This implies

$$T_1 = -\frac{1}{2} \sum_{j=1}^I \sum_{k=1}^I \beta_{j,k} f_j^n f_k^n \Delta x_j \Delta x_k. \quad (20)$$

Using the above equation in (15) and after simplification, we reach

$$\begin{aligned} \mu_0(t^{n+1}) &= \mu_0(t^n) + \left[e^{-K_1 t^n} - e^{-K_1 t^{n+1}} \right] \sum_{i=1}^I g(x_i, 0) \Delta x_i \\ &\quad - \frac{1}{2} \sum_{j=1}^I \sum_{k=1}^I \beta_{j,k} f_j^n f_k^n \Delta x_j \Delta x_k. \end{aligned} \quad (21)$$

Hence, the formulation (11) conserves the zeroth order moment, that is, it preserves the total number of particles in the system at each time step. \square

Let us now provide the theoretical proof of non-conservation of mass for the formulation (11) in the following Proposition 2.

Proposition 2. *The discrete formulation (11) does not preserve the total mass in the system.*

Proof. Multiplying Eq. (11) by $x_i \Delta x_i$ and summing over all i , the left hand side gives the first order moment $\mu_1(t)$ at time t^{n+1} and the right hand side can be evaluated to:

$$\mu_1(t^{n+1}) = \sum_{i=1}^I f_i^n x_i \Delta x_i + \sum_{i=1}^I x_i g(x_i, 0) \Delta x_i K_1 \int_{t^n}^{t^{n+1}} e^{-K_1 t} dt + \Delta t^n T_2,$$

where

$$T_2 = \frac{1}{2} \sum_{i=1}^I \sum_{(j,k) \in \Theta^i} x_i \beta_{j,k} f_j^n f_k^n \Delta x_j \Delta x_k - \sum_{i=1}^I \sum_{j=1}^I x_j \beta_{i,j} f_i^n f_j^n \Delta x_i \Delta x_j. \quad (22)$$

For proving mass conservation, it is needed to prove that $T_2 = 0$.

Interchanging i to j and j to k in the second term of the above equation leads to

$$T_2 = \frac{1}{2} \sum_{i=1}^I \sum_{(j,k) \in \Theta^i} x_i \beta_{j,k} f_j^n f_k^n \Delta x_j \Delta x_k - \sum_{j=1}^I \sum_{k=1}^I x_j \beta_{i,j} f_i^n f_j^n \Delta x_j \Delta x_k. \quad (23)$$

This further simplifies to

$$T_2 = \frac{1}{2} \sum_{i=1}^I \sum_{(j,k) \in \Theta^i} (x_i - x_j) \beta_{j,k} f_j^n f_k^n \Delta x_j \Delta x_k. \quad (24)$$

This implies

$$T_2 \neq 0.$$

Hence, the formulation defined in Eq. (11) does not hold the mass conservation law. \square

From the above proof, it can be observed that some corrections have to be made in the formulation (11) to preserve the total mass in the system. The finite volume approach is based on the idea that micelles are clustered on the pivot of the cell. However, it is unlikely that after the coagulation of two micelles, the size of the new micelle will coincide with the pivot of another cell. This gives three possibilities depending on whether the coagulated micelle falls on the pivot of a cell or not:

- **Possibility 1:** The coagulated micelle ($x_j + x_k$) lies between the lower boundary and pivot of the i th cell, that is, $x_{i-1/2} \leq x_j + x_k < x_i$.
- **Possibility 2:** The coagulated micelle ($x_j + x_k$) exactly falls on the pivot of the i th cell, that is, $x_j + x_k = x_i$.
- **Possibility 3:** The coagulated micelle ($x_j + x_k$) lies between the pivot and upper boundary of the i th cell, that is, $x_i < x_j + x_k \leq x_{i+1/2}$.

The graphical representation of all possibilities is demonstrated in Fig. 4.

In order to translate the aforementioned concept mathematically, the following correction factor is added to the formulation to help in

capturing the total mass in the system consistently:

$$\Phi_{j,k}^i = \begin{cases} \frac{x_j + x_k}{x_i}, & \text{for } x_j + x_k \neq x_i \\ 1, & \text{for } x_j + x_k = x_i, \\ 0, & \text{for } x_j + x_k < x_{min} \text{ or } x_j + x_k > x_{max}. \end{cases} \quad (25)$$

It is worth noting that the addition of this weight deteriorates the preservation of the zeroth order moment. After introducing the correction factor in the formulation (11), the finite volume approach takes the following form:

$$\begin{aligned} f_i^{n+1} &= f_i^n + \Delta t^n \left(g(x_i, 0) K_1 \int_{t^n}^{t^{n+1}} e^{-K_1 t} dt \right. \\ &\quad \left. + \frac{1}{2} \sum_{(j,k) \in \Theta^i} \beta_{j,k} f_j^n f_k^n \frac{\Delta x_j \Delta x_k}{\Delta x_i} \Phi_{j,k}^i - \sum_{j=0}^I \beta_{i,j} f_i^n f_j^n \Delta x_j \right). \end{aligned} \quad (26)$$

Our next major aim is to show that the finite volume approach (26) preserves mass.

2.2. Mass preservation law

Proposition 3. *The discrete formulation (26) preserves total mass in the presence of correction factor $\Phi_{j,k}^i$.*

Proof. Multiplying Eq. (26) by $x_i \Delta x_i$ and summing over all i , the left hand side gives the first order moment ($\mu_1(t)$) at time t^{n+1} , and the right hand side can be evaluated to:

$$\mu_1(t^{n+1}) = \sum_{i=1}^I f_i^n x_i \Delta x_i + \sum_{i=1}^I x_i g(x_i, 0) \Delta x_i K_1 \int_{t^n}^{t^{n+1}} e^{-K_1 t} dt + \Delta t^n T, \quad (27)$$

where

$$T = \frac{1}{2} \sum_{i=1}^I \sum_{(j,k) \in \Theta^i} \beta_{j,k} f_j^n f_k^n \Delta x_j \Delta x_k (x_j + x_k) - \sum_{i=1}^I \sum_{j=1}^I x_i \beta_{i,j} f_i^n f_j^n \Delta x_i \Delta x_j. \quad (28)$$

To conserve mass, we require $T = 0$.

Let us simplify the above equation by rewriting it as follows:

$$\begin{aligned} T &= \frac{1}{2} \sum_{i=1}^I \sum_{(j,k) \in \Theta^i} x_j \beta_{j,k} f_j^n f_k^n \Delta x_j \Delta x_k + \frac{1}{2} \sum_{i=1}^I \sum_{(j,k) \in \Theta^i} x_k \beta_{j,k} f_j^n f_k^n \Delta x_j \Delta x_k \\ &\quad - \sum_{i=1}^I \sum_{j=1}^I x_i \beta_{i,j} f_i^n f_j^n \Delta x_i \Delta x_j. \end{aligned} \quad (29)$$

Interchanging j and k in the second term of the above equation leads to

$$T = \sum_{i=1}^I \sum_{(j,k) \in \Theta^i} x_j \beta_{j,k} f_j^n f_k^n \Delta x_j \Delta x_k - \sum_{i=1}^I \sum_{j=1}^I x_i \beta_{i,j} f_i^n f_j^n \Delta x_i \Delta x_j. \quad (30)$$

Use the same argument similar to Proposition 1, the summation $\sum_{i=1}^I \sum_{(j,k) \in \Theta^i}$ exhibits the sum of all cells having indices j and k that intersect with the cell of index i . Therefore, it can also be written as

$$\sum_{i=1}^I \sum_{(j,k) \in \Theta^i} = \sum_{j=1}^I \sum_{k=1}^I.$$

It can be further evaluated to

$$T = \sum_{j=1}^I \sum_{k=1}^I x_j \beta_{j,k} f_j^n f_k^n \Delta x_j \Delta x_k - \sum_{i=1}^I \sum_{j=1}^I x_i \beta_{i,j} f_i^n f_j^n \Delta x_i \Delta x_j. \quad (31)$$

Now change the indices i to j and j to k in the second term of the above relation:

$$T = \sum_{j=1}^I \sum_{k=1}^I x_j \beta_{j,k} f_j^n f_k^n \Delta x_j \Delta x_k - \sum_{j=1}^I \sum_{k=1}^I x_j \beta_{j,k} f_j^n f_k^n \Delta x_j \Delta x_k. \quad (32)$$

This implies

$$T = 0.$$

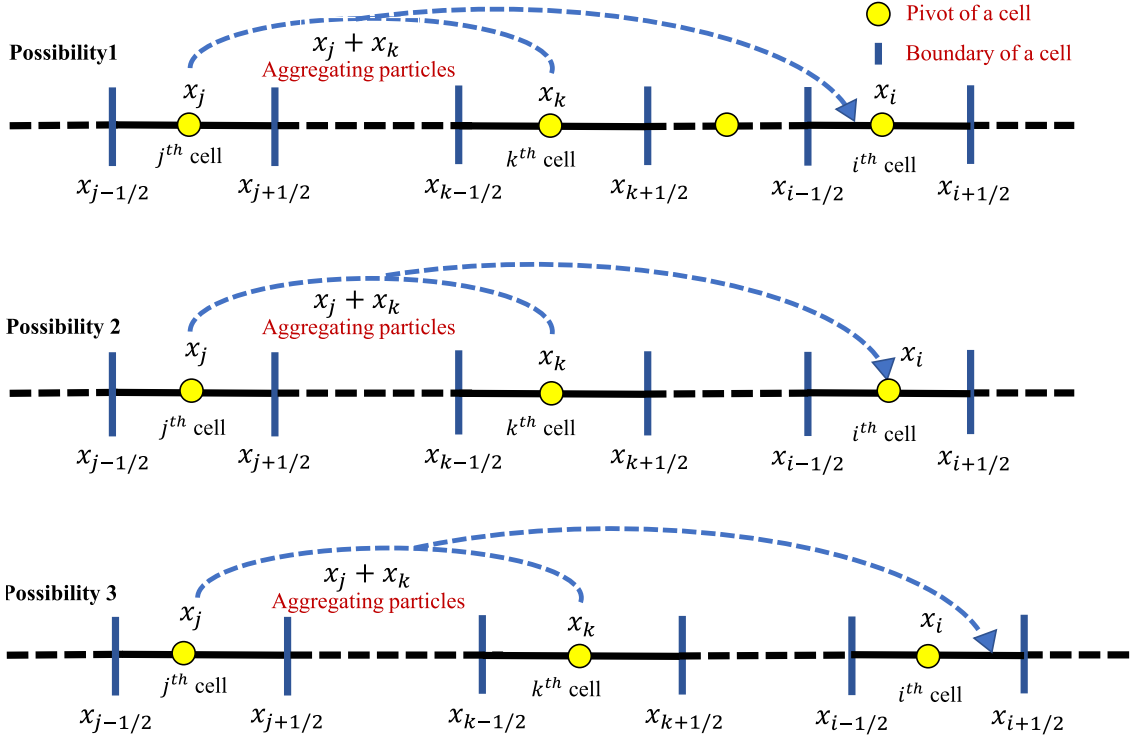


Fig. 4. Three basic possibilities where the coagulated micelles fall in the i th cell.

Finally, from Eq. (27), we obtain

$$\mu_1(t^{n+1}) = \mu_1(t^n) + \sum_{i=1}^I f_i^n x_i \Delta x_i + \sum_{i=1}^I x_i g(x_i, 0) \Delta x_i K_1 \int_{t^n}^{t^{n+1}} e^{-K_1 t} dt. \quad (33)$$

After simplification, it leads to

$$\mu_1(t^{n+1}) = \mu_1(t^n) + \left[e^{-K_1 t^n} - e^{-K_1 t^{n+1}} \right] \sum_{i=1}^I x_i g(x_i, 0) \Delta x_i, \quad (34)$$

which is same as Eq. (13). Hence, the total mass is preserved by this method. \square

Proposition 4. The correction factor $\Phi_{j,k}^i$ defined in (25) is unity for the uniform grid with $x_i = ip$ where p is a positive number.

Proof. For a uniform grid, the boundaries of all cells are equidistant. We can construct a uniform grid with $x_i = ip$ where p is a positive number.

This implies the coagulated micelle's volume is $x_j + x_k = (j+k)p = Mp$ for an integer M . Now for this uniform grid, the coagulated micelle ($x_j + x_k$) will fall exactly on the pivot of the cell $i = M$. This means $j+k=i$. Hence from Eq. (25), $\Phi_{j,k}^i = 1$. \square

Important note: It is worth noting here that Proposition 4 does not hold for an arbitrary uniform grid with $x_i = ip + q$ where p and q are both positive numbers.

2.3. CFL condition for positive solution

Since the new proposed scheme is an explicit time-stepping scheme, some care has to be taken with respect to the positivity of the approximate solution. Consider the positive initial data $f_i^0 > 0$ for all i . In order to ensure positivity of the numerical solution, a stability (CFL) condition for the time step similar to Forestier-Coste and Mancini [25] is defined. The CFL condition in this case is given by

$$\Delta t^n < \min_i \left(\left| \frac{f_i^n}{S_i^n + B_i^n - D_i^n} \right| \right), \quad (35)$$

where the terms B_i^n and D_i^n denote the discrete birth and death of particles in the i th cell, given as

$$B_i^n = \frac{1}{2} \sum_{(j,k) \in \Theta^i} \beta_{j,k} f_j^n f_k^n \frac{\Delta x_j \Delta x_k}{\Delta x_i} \Phi_{j,k}^i,$$

and

$$D_i^n = \sum_{j=1}^I \beta_{i,j} f_i^n f_j^n \Delta x_j.$$

Hence, under the restriction (35) on the time step Δt^n , the numerical results will be positive provided positivity is ensured in the initial data.

3. Numerical testing and discussion

The new approach has been tested in terms of integral moments and number of particles in each cell against newly developed analytical solutions corresponding to both non-gelling and gelling kernels. The comparison is conducted for an exponential initial condition $f(x, 0) = e^{-x}$ and $g(x, 0) = f(x, 0)$ for simplicity. The analytical solutions for the different order moments for both non-gelling and gelling kernels are listed in Table A.3. All the simulations were carried out using MATLAB-2021b academic version on a i7-1165G7 @2.80 GHz 11th generation Intel CPU and 16 GB RAM. The non uniform computational domain is discretized into I non uniform subintervals using the geometric recurrence relation $x_{i+1/2} = r x_{i-1/2}$.

The relative errors in the moments are calculated using the following relation

$$\sigma_i(t) = \left| \frac{m_i^{ana} - m_i^{num}}{m_i^{ana}} \right|. \quad (36)$$

for different grids at the end time. Here, m_i^{ana} and m_i^{num} denote the i th analytical and numerical moments, respectively.

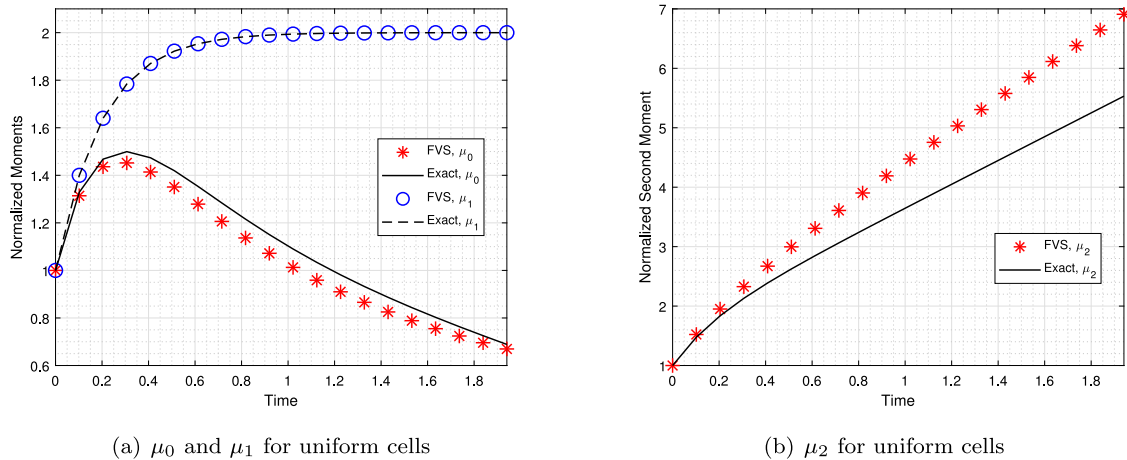


Fig. 5. Evolution of different moments for the constant kernel $\beta(x, y) = 1$ with $K_1 = 5$ for a uniform grid with 1000 cells.

3.1. Non-gelling constant kernel

Let us begin the testing by considering the constant kernel $\beta(x, y) = 1$. We consider a computational domain with the lower limit ($x_{min} = 10^{-2}$) and the upper limit ($x_{max} = 10^3$) having 1000 uniform cells. The other computational grids that we consider have 30 or 60 cells with logarithmic spacing between the same lower (10^{-2}) and upper (10^3) bounds. Due to non-availability of analytical (or exact) solutions for the number density functions, the accuracy of the method has been tested by deriving solutions for the moments. The simulations are obtained until time $t = 2$ for $K_1 = 5$ and $K_1 = 10$. Testing is done by comparing the numerical solution against the exact zeroth, first and second order moments provided in Appendix (Table A.3).

The numerical results for the moments with a uniform grid with 1000 cells are presented in Fig. 5. Despite the adherence to the mass preservation law, it is evident that the zeroth and second-order moments deviate significantly from the exact values despite the refined grid. Enhancing these results necessitates the use of an even more refined grid, thereby increasing computational costs. However, when employing a non-uniform grid with 30 cells, the obtained results are highly accurate in comparison to those with a uniform grid (refer to Fig. 6). Consequently, we have opted for the use of only a non-uniform grid for the remainder of the study.

It can be seen from Figs. 6(a) and 6(b) that the zeroth order moments are well predicted by the proposed approach, but the numerical approach over-predicts the analytical solutions at the end time. It is worth noting that the zeroth order moment, which represents the number of coagulated micelles, first increases at early times due to proteolysis. The first order moments illustrated in Figs. 6(a) and 6(b) increase over time as a result of the enzymatic proteolysis (first phase) of the coagulation process before significant coagulation begins. It is important to note that after the first phase ends (around time $t = 1$), the overall mass of the coagulated micelles does not change over time. In addition, the second order moments are illustrated in Figs. 6(c) and 6(d). Fig. 6(c) reveals that the new numerical approach (with 30 cells) over predicted the second order moment and deviates slightly from the exact moment. However, once a refined grid of 60 cells is used to calculate the second order moment, the accuracy increases and matches well with the exact moment (refer to Fig. 6(d)).

The number density distributions of the coagulated micelles for the first-two phases of the enzymatic coagulation process calculated numerically are demonstrated in Figs. 6(e) and 6(f) for 30 and 60 cells, respectively at different times. The relative errors (36) calculated for different K_1 values are listed in Table 1. It is worth noting that as the refined grid is used, the errors in moments are decreased and can be

Table 1

Error analysis of the moments at end time for non-gelling constant kernel.

m_i	$K_1 = 5$		$K_1 = 10$	
	30 cells	60 cells	30 cells	60 cells
m_0	0.0122	0.0090	0.0038	0.0027
m_1	6.14E-7	3.81E-7	1.25E-6	5.97E-7
m_2	0.0241	0.0070	0.0250	0.0073

reduced to a desired level by considering a more refined grid but at an increased computational cost.

In order to understand the effect of the constant K_1 (used to define the enzymatic proteolysis), the numerical results obtained by considering $K_1 = 10$ are graphically shown in Fig. 7. The initial increase in the number of coagulating micelles occurs faster than in the previous case where $k = 5$ was considered (refer to Figs. 6(a) and 6(b)). The first order moment does not alter much for different values of K_1 as shown in Figs. 6(a), 6(b), 7(a) and 7(b). It is worth noting that for $K_1 = 10$, the total mass increases to a steady value in a shorter time period ($t = 0.55$) than with $K_1 = 5$ (at $t = 1$). The differences in the behaviour of the distributions can also be observed for different values of K_1 and grids with various cell sizes (see Figs. 6(e), 6(f), 7(e) and 7(f)). These figures show the role of the enzymatic proteolysis rate constant K_1 on the overall progress of the coagulation process.

3.2. Gelling sum kernel

Now we extend the comparison by considering a strongly size-dependent gelling kernel of the form $\beta(x, y) = x + y$. The computational domain $[10^{-2} 10^3]$ is divided into 60 non-uniform cells. The simulation is run until $t = 1.27$ and the values of K_1 are considered to be 5 and 10. The comparison of the different moments obtained using the finite volume scheme are compared against newly derived analytical solutions. The analytical moments are computed using Picard's method which will be provided in a subsequent article, however, the expressions of different moments are provided in Table A.4 of Appendix. For comparing the zeroth and second order moments, the 10th iteration result of Picard's method is considered.

Fig. 8 presents the comparison of the numerical and exact solutions for the different moments for the sum kernel. Once again the numerical approach captures the zeroth and first order moments with higher precision, as depicted in Figs. 8(a) and 8(b). In addition, the second order moments corresponding to $K_1 = 5$ and $K_1 = 10$ are shown in Figs. 8(c) and 8(d), respectively. Even though no specific measures have been taken to compute the second order moments accurately, the numerical approach predict these moments with reasonable accuracy.

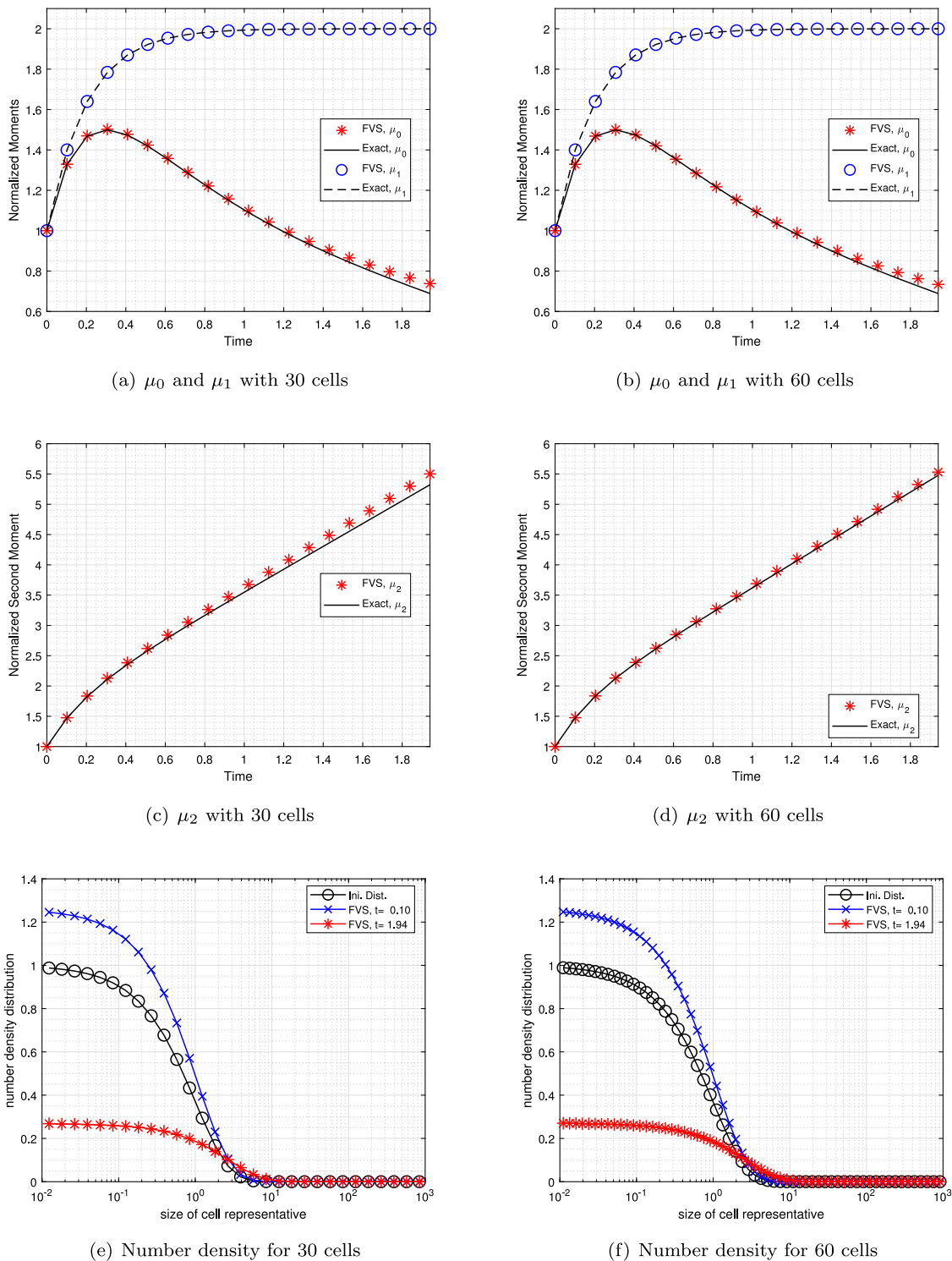


Fig. 6. Evolution of different moments and the number density for the constant kernel $\beta(x, y) = 1$ with $K_1 = 5$.

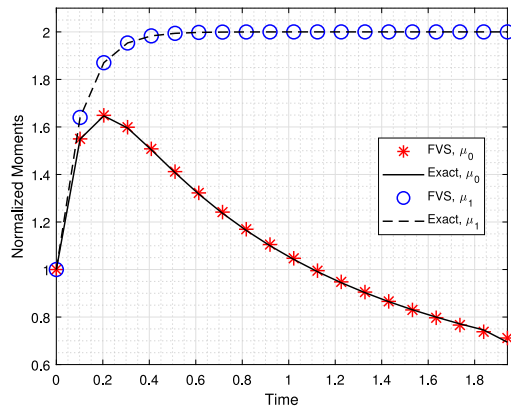
Moreover, the number density distributions of the coagulated micelles is plotted against the size of the cell corresponding to $K_1 = 5$ and $K_1 = 10$ in Figs. 8(e) and 8(f). Once again the relative errors calculated for the gelling sum kernel listed in Table 2 shows that the errors reduced significantly when the simulation is run for a refined grid of 60 non-uniform cells compared to a coarse grid of 30 non-uniform cells.

In order to observe the gelling behaviour for the sum kernel, the simulation is run for an extended time (0 to 1.5) with 60 non-uniform cells. The results are shown in Fig. 9. One can see that mass loss starts

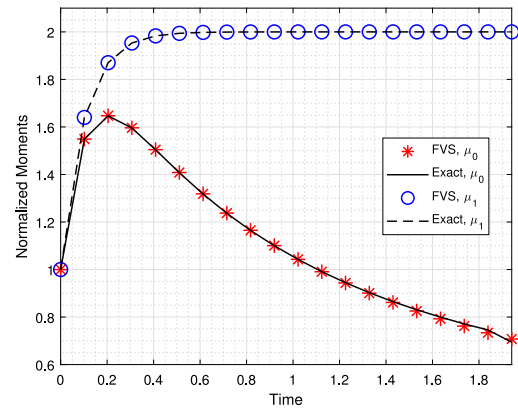
from $t = 1.25$. The effect of mass loss can also be seen in the zeroth moment. The accuracy can be improved by considering a more refined grid but at a higher computational cost.

3.3. Brownian kernel

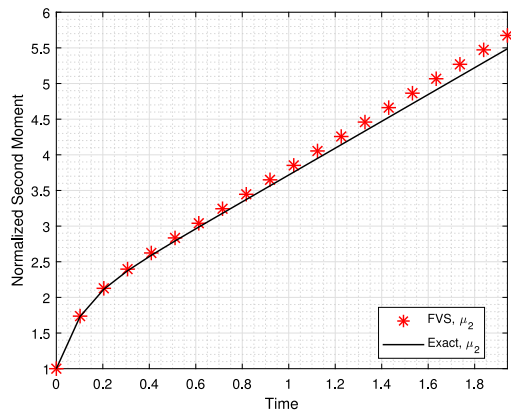
Here the numerical results are compared for a physically-relevant kernel known as the Brownian kernel of the form $\beta(x, y) = (x^{1/3} + y^{1/3})(x^{-1/3} + y^{-1/3})$ [34,35]. This kernel has been used in different applications related to pharmaceutical processes (see Ref. [36]



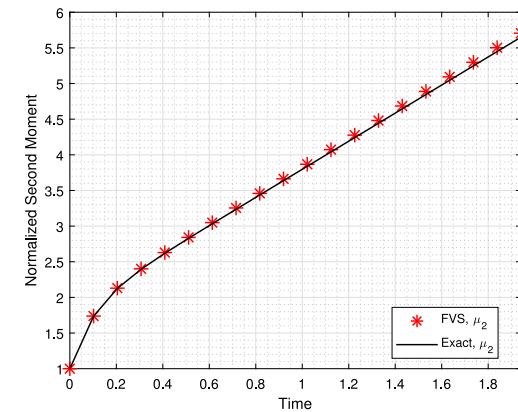
(a) μ_0 and μ_1 for 30 cells



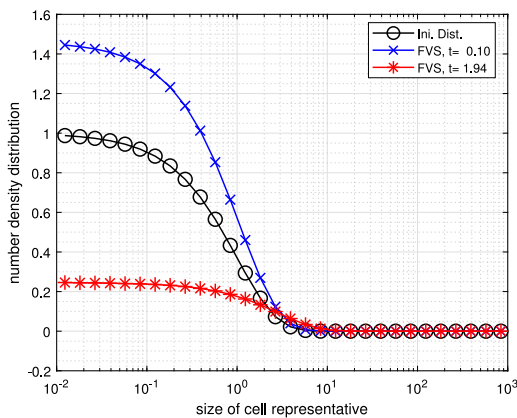
(b) μ_0 and μ_1 for 60 cells



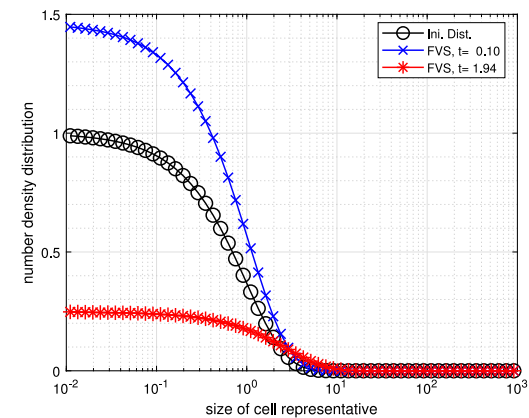
(c) μ_2 for 30 cells



(d) μ_2 for 60 cells



(e) Number density for 30 cells



(f) Number density for 60 cells

Fig. 7. Evolution of different moments and the number density for the constant kernel $\beta(x, y) = 1$ for $K_1 = 10$.

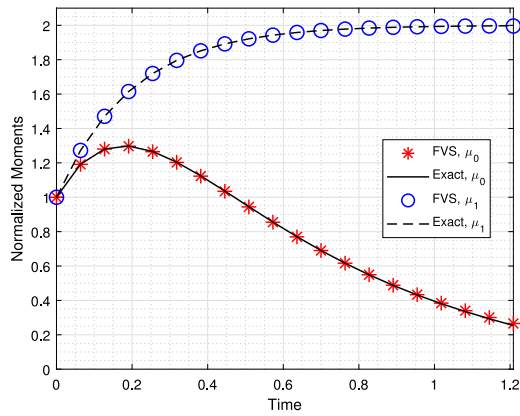
Table 2

Error analysis of the moments at end time for sum kernel.

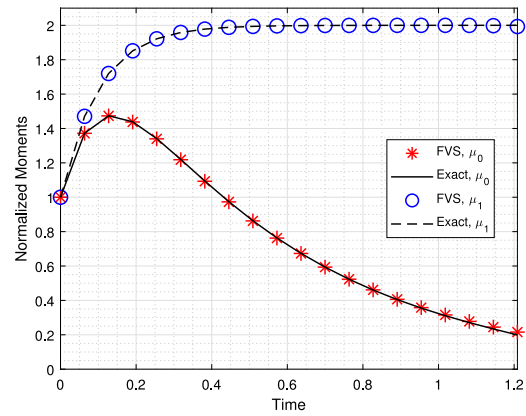
m_i	$K_1 = 5$		$K_1 = 10$	
	30 cells	60 cells	30 cells	60 cells
m_0	0.0145	0.0116	0.0157	0.0130
m_1	2.37E-4	1.06E-4	7.89E-4	3.95E-4
m_2	0.2007	0.1940	0.2156	0.2127

and therein). The simulation is run for a computational domain $[10^{-3} \ 10^5]$ having 60 non-uniform cells until $t = 2$. The values of the parameter K_1 are considered to be 5 and 10.

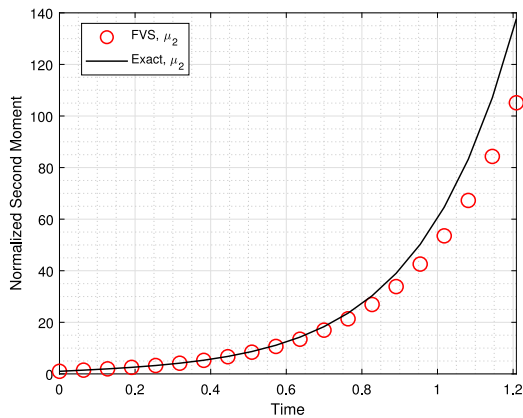
For this case, analytical solutions for the number density function and the corresponding moments are not possible to derive due to the complex nature of this kernel. However, the exact solution for the first order moment can be derived, which is similar to previous cases. The numerical results in terms of moments and distribution are provided in Fig. 10. The total mass in the system is consistently preserved by the new approach and overlaps with the exact result as demonstrated in



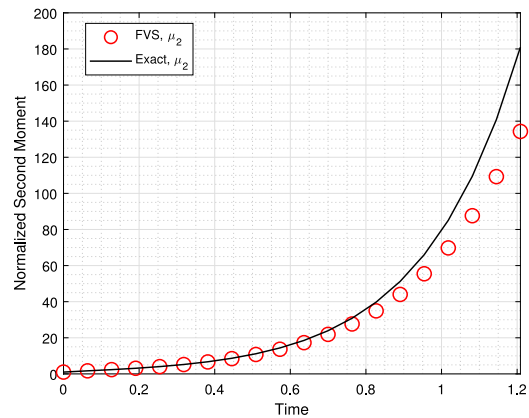
(a) μ_0 and μ_1 for $K_1 = 5$



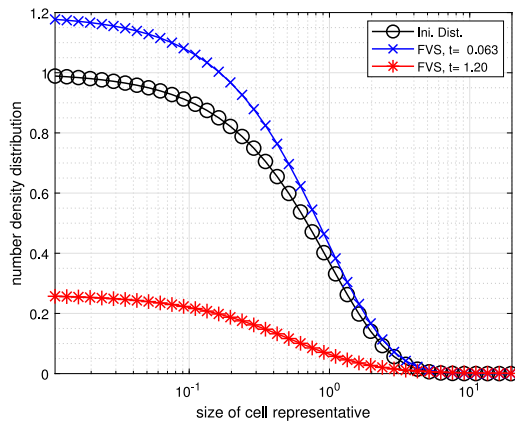
(b) μ_0 and μ_1 for $K_1 = 10$



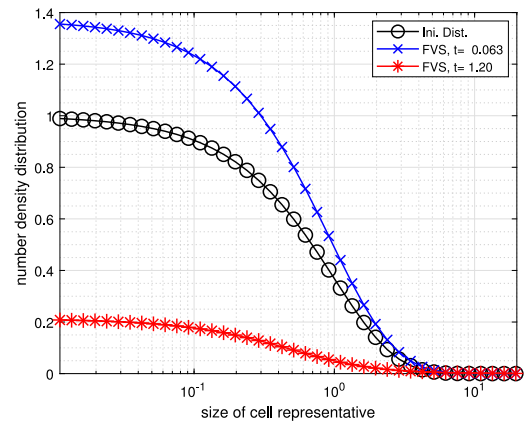
(c) μ_2 for $K_1 = 5$



(d) μ_2 for $K_1 = 10$



(e) Number density for $K_1 = 5$



(f) Number density for $K_1 = 10$

Fig. 8. Evolution of different moments and the number density for the sum kernel $\beta(x, y) = x + y$ and 60 non-uniform cells.

plots 10(a) and 10(b). The zeroth order moment, plotted in Figs. 10(a) and 10(b), follows similar trends as the previous cases. The behaviour of the zeroth order moment is quite similar to the sum kernel case, however, the first phase is shorter in time than it is with the sum kernel. The second order moments calculated by the new approach show linear growth with time (refer to Figs. 10(c) and 10(d)) for both values of K_1 . The coagulated micelle number density distribution computed using the new approach has been plotted in Figs. 10(e) and 10(f). The number distributions show similar trends as earlier cases.

From the discussion above, it has been shown that the proposed approach is flexible and robust to implement on both empirical and physically relevant kernels. The effect of K_1 on the distributions and their integral moments is discussed.

4. Final conclusions, remarks and future prospects

A new mass preserving approach based on the finite volume scheme has been developed for solving a rennet-coagulation equation arising

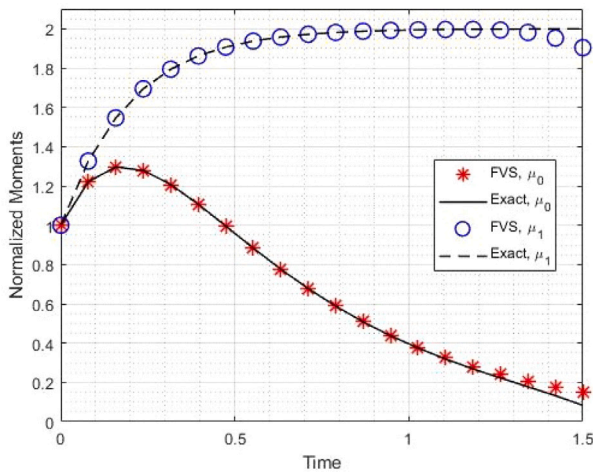


Fig. 9. Gelling behaviour using sum kernel $\beta(x, y) = x + y$ for 60 cells.

in the field of dairy science. The mathematical formulation of the new approach is simple and reliable to implement on any grid. The new approach was compared to newly derived analytical solutions for two types of kernels: gelling and non-gelling. Even though no explicit precision assessments were completed, it was proven that the novel approach calculated the zeroth and second order moments with good accuracy while using few cells. In other words, the idea of the new approach is based on conservation of the total mass in the system (rather than other moments). In addition, the number density distribution of coagulated micelles is also captured by the proposed approach. In addition to the constant and sum kernels, computational and analytical results are also compared for the physically-relevant Brownian kernel, which has been considered for modelling many processes in pharmaceutical sciences.

Even though the new approach captures the zeroth order moment well, conservation of the zeroth order moment is not guaranteed. In the future, We will therefore development an approach that preserves both zeroth and first order moments consistently. In addition, we will consider different expressions for the kinetics of proteolysis (for example second order kinetics) to see the impact of the kinetics on the size distribution of coagulated micelles. Due to the higher accuracy and efficiency of the proposed scheme, we will also extend this technique to track multiple properties of the system by considering a multidimensional equation [37,38].

CRedit authorship contribution statement

Mehakpreet Singh: Conceptualization, Formal analysis, Investigation, Methodology, Software, Validation, Visualization, Writing – original draft, Writing – review & editing. **Nikhil Sriwastav:** Formal analysis, Investigation, Methodology, Validation, Writing – original draft. **Orest Shardt:** Formal analysis, Investigation, Supervision, Validation, Writing – original draft, Writing – review & editing.

Declaration of competing interest

The authors declare that they have no known competing financial interests or personal relationships that could have appeared to influence the work reported in this paper.

Data availability

No data was used for the research described in the article.

Acknowledgement

This work has been supported by the Dairy Processing Technology Centre funded through Enterprise Ireland, Grant Agreement number: TC 2020 0028.

Appendix. Analytical solutions for different moments

Let us now derive the analytical solutions for a enzymatic coagulation process corresponding to the constant and sum kernels. For deriving the moments, we assume $g(x, 0) = f(x, 0) = \exp(-x)$. Integrate the original equation (1) with respect to variable x from 0 to ∞ , and after simplification we get the following relation:

$$\frac{d\mu_k(t)}{dt} = K_1 e^{-K_1 t} \int_0^\infty x^k f(x, 0) dx + \frac{1}{2} \int_0^\infty \int_0^\infty [(x + x')^k - x^k - x'^k] \times \beta(x, x') f(x', t) f(x, t) dx dx' \tag{A.1}$$

These equations in terms of $\mu_k(t)$ will be solved using Picard’s iterative technique.

For example, for the sum kernel $\beta(x', x', t) = \beta_0(t)(x + x')$ and $k = 0$, the above expression after simplification takes the following form:

$$\frac{d\mu_0(t)}{dt} = K_1 e^{-K_1 t} \mu_0(0) - \beta_0 \mu_1(0) [2 - e^{-K_1 t}] \mu_0(t) \tag{A.2}$$

Integrating with respect to t from 0 to t gives

$$m_0(t) = m_0(0) + K_1 m_0(0) \int_0^t e^{-K_1 t} dt - \beta_0 \mu_1(0) \times \int_0^t (2 - e^{-K_1 t} m_0)(t) dt \quad \text{for } i = 0, 1, 2, \dots \tag{A.3}$$

Implementing Picard’s iterative formula, we have

$$m_0^{i+1}(t) = m_0(0) + K_1 m_0(0) [1 - e^{-K_1 t}] - \beta_0 \mu_1(0) \int_0^t (2 - e^{-K_1 t}) m_0^i(t) dt \quad \text{for } i = 0, 1, 2, \dots \tag{A.4}$$

Here $m_0^0 = m_0(0)$, $m_1(0)$ and $m_2(0)$ denote the zeroth, first and second order moments, respectively at time $t = 0$. Similarly, for other values of k , the different order moments can be derived.

Table A.3

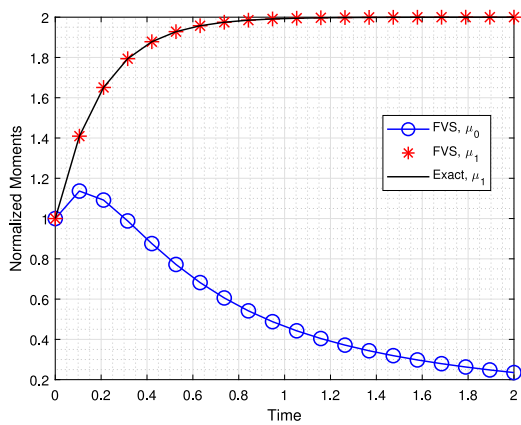
Exact solutions for zeroth, first and second order moments corresponding to constant kernel.

Second iteration of zeroth moment ($\mu_0(t)$)	$\frac{m_0(0)}{24K_1^2} \left(-m_0^3(0)K_1^2 t^3 \beta_0^3 + 12m_0^2(0)K_1^2 t^2 \beta_0^2 + 12m_0^3(0)e^{-K_1 t} K_1 t \beta_0^2 + 12m_0^2(0)e^{-K_1 t} \beta_0^2 + 6m_0(0)e^{-2K_1 t} K_1 \beta_0 - 48m_0(0)K_1^2 t \beta_0 - 12\beta_0^2 m_0^2(0) - 48m_0(0)e^{-K_1 t} K_1 \beta_0 + 42m_0(0)\beta_0 K_1 - 24e^{-K_1 t} K_1^2 + 48K_1^2 \right)$
First moment ($\mu_1(t)$)	$m_1(0)(2 - e^{-K_1 t})$
Second moment ($m_2(t)$)	$m_2(0)(2 - e^{-K_1 t}) + 4t + (1/(2K_1))(1 - e^{-2K_1 t}) - (4/(K_1))(1 - e^{-K_1 t})$

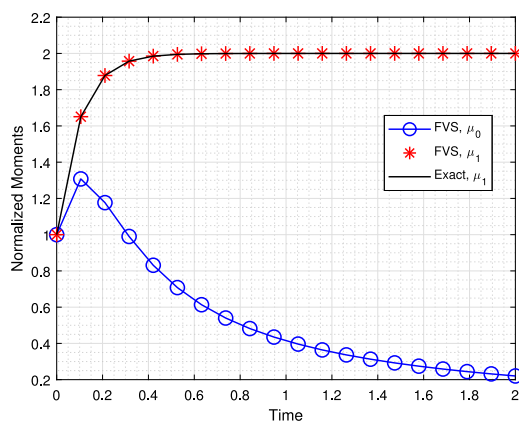
Table A.4

Exact solutions for zeroth, first and second order moments corresponding to sum kernel.

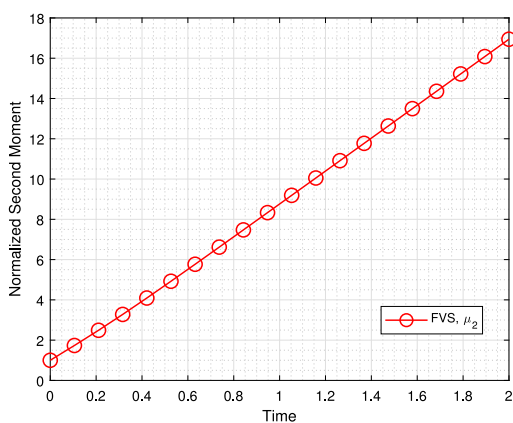
Second iteration of zeroth moment ($\mu_0(t)$)	$\frac{m_0(0)}{K_1^2} \left(2K_1^2 + 2K_1^2 t^2 + 0.5e^{-2K_1 t} K_1 + 2e^{-K_1 t} K_1 t - 4K_1^2 t + 0.5e^{-2K_1 t} - 4K_1 e^{-K_1 t} - 2K_1 t - e^{-K_1 t} + 3.5K_1 + 0.5 - K_1^2 e^{-K_1 t} \right)$
First moment ($\mu_1(t)$)	$m_1(0)(2 - e^{-K_1 t})$
Second iteration of second moment ($m_2(t)$)	$-\frac{m_2(0)}{K_1^2} \left(-8\beta_0^2 K_1^2 t^2 - 8e^{-K_1 t} K_1 t \beta_0^2 - 8\beta_0 K_1^2 t + 8\beta_0^2 t K_1 + e^{-K_1 t} K_1^2 + \beta_0 e^{-2K_1 t} K_1 - 2\beta_0^2 e^{-2K_1 t} - 2K_1^2 + 7K_1 \beta_0 - 2\beta_0^2 \right)$



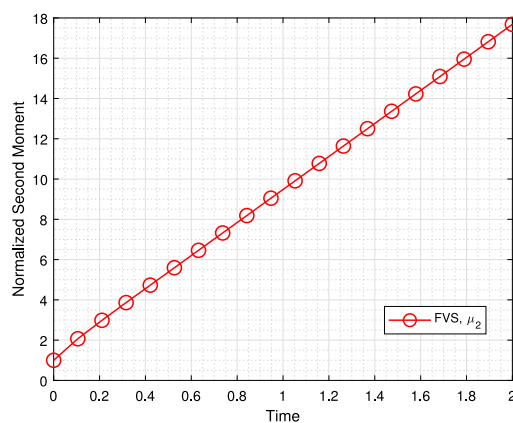
(a) μ_0 and μ_1 for $K_1 = 5$



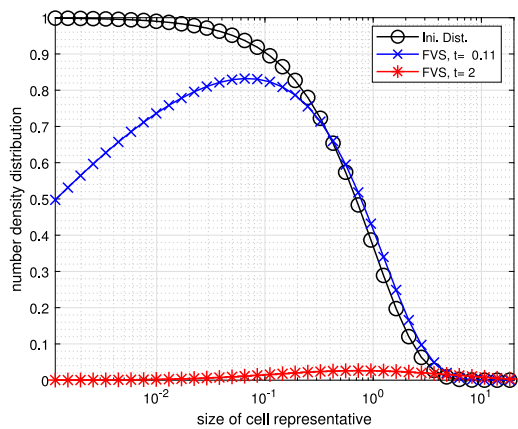
(b) μ_0 and μ_1 for $K_1 = 10$



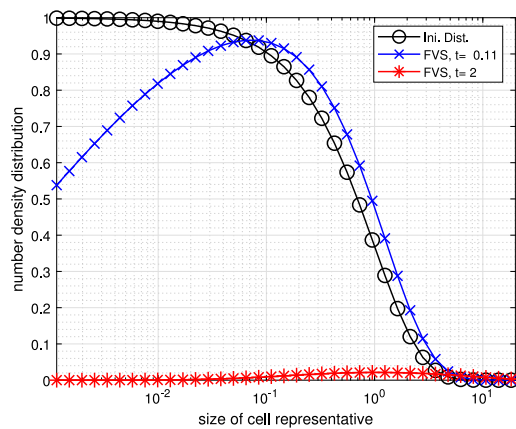
(c) μ_2 for $K_1 = 5$



(d) μ_2 for $K_1 = 10$



(e) Number density for $K_1 = 5$



(f) Number density for $K_1 = 10$

Fig. 10. Evolution of different moments and the number density for the Brownian kernel $\beta(x, y) = (x^{1/3} + y^{1/3})(x^{-1/3} + y^{-1/3})$.

References

[1] Holt Carl, Home David S. The hairy casein micelle: Evolution of the concept and its implications for dairy technology. *Neth Milk Dairy J* 1996;50:85–111.
 [2] Konuklar Gül, Gunasekaran Sundaram. Rennet-induced milk coagulation by continuous steady shear stress. *J Colloid Interface Sci* 2002;250(1):149–58.
 [3] Zhong Qixin, Daubert Christopher R. Kinetics of rennet casein gelation at different cooling rates. *J Colloid Interface Sci* 2004;279(1):88–94.
 [4] Payens TA. The enzyme-triggered coagulation of casein micelles. *Adv Colloid Interface Sci* 1989;30:31–69.

[5] Niki Ryoya, Kohyama Kaoru, Sano Yoh, Nishinari Katsuyoshi. Rheological study on the rennet-induced gelation of casein micelles with different sizes. *Polym Gels Netw* 1994;2(2):105–18.
 [6] Ismail Hamza Y, Singh Mehakpreet, Shirazian Saeed, Albadarin Ahmad B, Walker Gavin M. Development of high-performance hybrid ann-finite volume scheme (ann-fvs) for simulation of pharmaceutical continuous granulation. *Chem Eng Res Des* 2020;163:320–6.
 [7] Bilgili Ecevit, Scarlett B. Nonlinear effects in particulate processes. *Nonlinear Anal TMA* 2005;63(5–7):e1131–41.

- [8] Singh Mehakpreet, Walker Gavin. New discrete formulation for reduced population balance equation: an illustration to crystallization. *Pharm Res* 2022;39(9):2049–63.
- [9] Lin Shihong, Wiesner Mark R. Deposition of aggregated nanoparticles—a theoretical and experimental study on the effect of aggregation state on the affinity between nanoparticles and a collector surface. *Environ Sci Technol* 2012;46(24):13270–7.
- [10] Bellomo Nicola, Bellouquid Abdelghani. On the derivation of macroscopic hyperbolic equations for binary multicellular growing mixtures. *Comput Math Appl* 2009;57(5):744–56.
- [11] Nguyen Tan Trung, Laurent Frédérique, Fox Rodney O, Massot Marc. Solution of population balance equations in applications with fine particles: mathematical modeling and numerical schemes. *J Comput Phys* 2016;325:129–56.
- [12] McBride AC, Smith AL, Lamb W. Strongly differentiable solutions of the discrete coagulation–fragmentation equation. *Physica D* 2010;239(15):1436–45.
- [13] Niethammer Barbara, Velazquez Juan JL. Self-similar solutions with fat tails for Smoluchowski’s coagulation equation with locally bounded kernels. *Comm Math Phys* 2013;318(2):505–32.
- [14] Rezakhanlou Fraydoun. Moment bounds for the solutions of the Smoluchowski equation with coagulation and fragmentation. *Proc R Soc Edinburgh Sect A: Math* 2010;140(5):1041–59.
- [15] Melzak ZA. A scalar transport equation. *Trans Amer Math Soc* 1957;85(2):547–60.
- [16] Scott William T. Analytic studies of cloud droplet coalescence I. *J Atmos Sci* 1968;25(1):54–65.
- [17] Dubovskii PB, Galkin VA, Stewart IW. Exact solutions for the coagulation-fragmentation equation. *J Phys A: Math Gen* 1992;25(18):4737.
- [18] Kaur Gurmeet, Singh Randhir, Singh Mehakpreet, Kumar Jitendra, Matsoukas Themis. Analytical approach for solving population balances: a homotopy perturbation method. *J Phys A* 2019;52(38):385201.
- [19] Yadav Sonia, Keshav Somveer, Singh Sukhjit, Singh Mehakpreet, Kumar Jitendra. Homotopy analysis method and its convergence analysis for a nonlinear simultaneous aggregation-fragmentation model. *Chaos Solitons Fractals* 2023;177:114204.
- [20] Yadav Nisha, Das Ashok, Singh Mehakpreet, Singh Sukhjit, Kumar Jitendra. Homotopy perturbation method and its convergence analysis for nonlinear collisional-fragmentation equations. *Proc R Soc Lond Ser A Math Phys Eng Sci* 2023;479(2279):20230567.
- [21] De Tarun, Das Ashok, Singh Mehakpreet, Kumar Jitendra. Enhancing efficiency in particle aggregation simulations: Coarse-grained particle modeling in the DEM-PBM coupled framework. *Comput Methods Appl Mech Engrg* 2023;417:116436.
- [22] Majumder Aniruddha, Kariwala Vinay, Ansumali Santosh, Rajendran Arvind. Lattice Boltzmann method for population balance equations with simultaneous growth, nucleation, aggregation and breakage. *Chem Eng Sci* 2012;69(1):316–28.
- [23] Filbet Francis, Laurençot Philippe. Numerical simulation of the Smoluchowski coagulation equation. *SIAM J Sci Comput* 2004;25(6):2004–28.
- [24] Bourgade Jean-Pierre, Filbet Francis. Convergence of a finite volume scheme for coagulation-fragmentation equations. *Math Comp* 2008;77(262):851–82.
- [25] Forestier-Coste Louis, Mancini Simona. A finite volume preserving scheme on nonuniform meshes and for multidimensional coalescence. *SIAM J Sci Comput* 2012;34(6):B840–60.
- [26] Singh Mehakpreet, Ismail Hamza Y, Matsoukas Themis, Albadarin Ahmad B, Walker Gavin. Mass-based finite volume scheme for aggregation, growth and nucleation population balance equation. *Proc R Soc Lond Ser A Math Phys Eng Sci* 2021;475(2231):20190552.
- [27] Singh Mehakpreet. New finite volume approach for multidimensional Smoluchowski equation on nonuniform grids. *Stud Appl Math* 2021;147(3):955–77.
- [28] Kumar Jitendra, Warnecke Gerald. Convergence analysis of sectional methods for solving breakage population balance equations-II: the cell average technique. *Numer Math* 2008;110(4):539–59.
- [29] Saha Jitraj, Singh Mehakpreet. Rate of convergence and stability analysis of a modified fixed pivot technique for a fragmentation equation. *Numer Math* 2023;153(2–3):531–55.
- [30] Singh Mehakpreet, Ranade Vivek, Shardt Orest, Matsoukas Themis. Challenges and opportunities concerning numerical solutions for population balances: a critical review. *J Phys A* 2022;55(38):383002.
- [31] Hyslop Douglas B. Enzyme-induced coagulation of casein micelles: a number of different kinetic models. *J Dairy Res* 1993;60(4):517–33.
- [32] Lomholt S B, Worning P, Øgden L, Qvist K B, Hylsop D B, Bauer R. Kinetics of the renneting reaction followed by measurement of turbidity as a function of wavelength. *J Dairy Res* 1998;65(4):545–54.
- [33] Kumar Jitendra, Kaur Gurmeet, Tsotsas Evangelos. An accurate and efficient discrete formulation of aggregation population balance equation. *Kinet Relat Models* 2016;9(2):373–91.
- [34] Yadav Nisha, Singh Mehakpreet, Singh Sukhjit, Singh Randir, Kumar Jitendra. A note on homotopy perturbation approach for nonlinear coagulation equation to improve series solutions for longer times. *Chaos Solitons Fractals* 2023;173:113628.
- [35] Ahrens Robin, Le Borne Sabine. Reconstruction of low-rank aggregation kernels in univariate population balance equations. *Adv Comput Math* 2021;47(3):1–15.
- [36] Singh Mehakpreet, Shirazian Saeed, Ranade Vivek, Walker Gavin M, Kumar Ashish. Challenges and opportunities in modelling wet granulation in pharmaceutical industry—A critical review. *Powder Technol* 2022;117380.
- [37] Singh Mehakpreet, Ismail Hamza Y, Singh Randhir, Albadarin Ahmad B, Walker Gavin. Finite volume approximation of nonlinear agglomeration population balance equation on triangular grid. *J Aerosol Sci* 2019;137:105430.
- [38] Singh Mehakpreet, Vuik Kees, Kaur Gurmeet, Bart Hans-Jörg. Effect of different discretizations on the numerical solution of 2D aggregation population balance equation. *Powder Technol* 2019;342:972–84.